sustainability

MDPI

Article

Transformation of Urban Surfaces and Heat Islands in Nanjing during 1984–2018

Yanxia Li [1,2], Xinkai Zhang [3,4], Sijie Zhu [1,2], Xiaoyu Wang [1,2], Yongdong Lu [1,2], Sihong Du [3,4] and Xing Shi [1,3,4,*]

1 School of Architecture, Southeast University, Nanjing 210096, China; liyanxia@seu.edu.cn (Y.L.); zhusijie@seu.edu.cn (S.Z.); w_xiaoyu@seu.edu.cn (X.W.); ydlu@seu.edu.cn (Y.L.)
2 Key Laboratory of Urban and Architectural Heritage Conservation, Ministry of Education, Nanjing 210096, China
3 College of Architecture and Urban Planning, Tongji University, Shanghai 200092, China; zhang_xinkai@seu.edu.cn (X.Z.); 1701430@stu.neu.edu.cn (S.D.)
4 Key Laboratory of Ecology and Energy-Saving Study of Dense Habitat (Tongji University), Ministry of Education, Shanghai 200092, China
* Correspondence: 20101@tongji.edu.cn; Tel.: +86-159-0519-1490

Received: 3 July 2020; Accepted: 10 August 2020; Published: 12 August 2020

Abstract: One of the many consequences of urbanization is the expansion of cities into rural areas, which leads to the transformation of lands from natural surfaces to developed surfaces. It is widely considered an established fact that urbanization generally increases the heat island effect. The objective of this study is to understand the pattern of urban surface transformation in the city of Nanjing since 1980 and to find, if any, the correlation between such transformation and the urban heat island effect. The supervised classification technique was used to analyze the remote sensing data obtained from Landsat to identify the different kinds of underlying surfaces. Land surface temperatures were calculated using a subset of Landsat data. The correlation between the transformation of underlying surfaces and the heat island effect was established through analytical and statistical approaches. The results clearly show that the proportion of developed surfaces has been steadily rising in Nanjing in the past 30 years and that the urban heat island effect is positively correlated with the expansion of hard pavement and the deterioration of green surfaces and water bodies considering the general trend.

Keywords: urban underlying surface; supervised classification; GIS; urban heat island

1. Introduction

Currently, more than half of the world's population live in cities, while the rate of urbanization is still increasing. Experts estimate that urban residents could account for 60% of the world's total population by 2030, which makes urbanization one of the few events that have a significant influence on the world [1]. After more than two decades of a headlong rush to transform China from an autarkic centrally planned economy into a limited open-market economy, China has gradually entered the process of rapid urbanization. The process of urbanization has always closely cooperated with the expansion of urban land use. One of the primary indicators of urbanization expansion is the spreading of urban developed land, which leads to an increase in impervious underlying surfaces and the decrease in natural underlying surfaces such as green lands, water bodies, and so forth.

The underlying surface refers to the earth's surface in direct contact with the lower atmosphere. The lower layer of the atmosphere is the earth's surface, known as the underlying surface of the atmosphere. The underlying surface, including topography, geology, soil, vegetation, and buildings, has a significant impact on the climate. The urban underlying surface refers to the part of the city

in direct contact with the atmosphere. There are a large number of buildings in the city, which are in direct contact with the lower atmosphere and change the underlying surface. Urban underlying surface changes will result in an urban climate island, such as a heat island or cool island. The structure and properties of the urban underlying surface are the main factors that affect the urban heat island effect, which forms the basement of urban heat island. To study the relationship between the type of underlying surface and the urban heat island effect, a variety of urban underlying surface types need to be extracted. The method of urban underlying surface type extraction is to use the visible light near-infrared band for remote sensing image classification.

There are many positive effects of urbanization, such as providing a sound infrastructure, creating more employment opportunities, and raising the efficiency of industrial production. However, in the process of continuous urbanization, the quality of environment is deteriorating as a consequence of noise pollution, light pollution, haze, and so forth. Additionally, the heat island effect is one of the outstanding environmental problems faced by cities.

The urban heat island (UHI) refers to the phenomenon that the temperature in a city is apparently higher than that of a rural area. In a surface layer temperature map, the temperature change in rural areas is mild, while the urban areas are high-temperature regions, like an island extruding from the sea; as such an island represents the areas of high-temperature city, such city is vividly called an UHI. The UHI effect can be divided into surface heat island and canopy heat island. The UHI often mentioned is the canopy heat island, which is the difference between the air temperature in the urban areas and the rural temperature. This paper studies the former, the difference between the surface temperature in the urban areas and the rural temperature.

In the process of expansion of cities, the UHI effect attracts ever-increasing attention, and alleviating the heat island effect has great significance in energy saving and urban planning. Subconsciously, many residents believe that larger scale cities have a stronger heat island effect. After a preliminary understanding of these phenomena, this study reviews the historical changes of the underlying surface and the heat island effect of the city and explores whether the hypothesis of the relationship between the underlying surface and the heat island effect can be established. In this study, a supervised method is adopted to extract underlying surface type. This method has high accuracy and low recapitulation rate. A mono-window algorithm method is used to retrieve the land-surface temperature, as it can retrieve the temperature without atmospheric correction. Meanwhile, this research also defined a method to determine urban and rural areas.

2. Literature Review

The spreading of urban developed land and the decrease in natural underlying surfaces are the two primary indicators of urbanization. Currently, few pieces of research directly studied the historical changes of the underlying surface of Nanjing. Meanwhile, scholars have done a lot of studies on urban expansion. A study conducted a comparative analysis of 30-year urban expansion patterns and rates among six metropolises from both China and the USA [2]. The study was based on time-series impervious surface area data extracted from multi-temporal Landsat images using the linear spectral mixture analysis approach [2]. Yoonshin Kwak et al. evaluated whether the planning of 4 new Korean towns was reasonable through the quantification and impact analysis of the UHI [3]. Cai et al. studied the degree of coordination of land use and urbanization in Nanjing based on the annual data of land use and urbanization development [4]. Zhang measured the degree of coordination of land urbanization and population urbanization in Nanjing and proposed that the urbanization level of Nanjing from 1996 could be divided into three stages: incoordination, less-coordination, and coordination [5]. In the research of the scale of urban expansion, Shi introduced reasons and motivations for the expansion of Nanjing in detail [6]. Wang presented the Nanjing urban expansion through studying the intensive land use in urbanization process [7]. Tu et al. analyzed the changes in the center of the mass of surface urban heat islands and the correlation between surface urban heat islands and urban expansion based on data from Nanjing in the past 10 years [8].

Research on the UHI effect can be divided into two categories. One is the measurement-based study of heat island effect, and the other is the theoretical analysis. There have been many measurement-based studies of the UHI. As early as 1818, Howard measured the UHI of London. Since then, other cities began to measure and report the UHI effect [9]. Wang et al. found that the ultra-high-emission cities and urban morphology affect the atmospheric circulation to a certain extent through the simulation analysis of UHI circulation and atmospheric circulation [10]. Streutker utilized satellite remote sensing to measure the heat island intensity of Houston, USA, and found that the average heat island intensity increased by 0.8 °C in the past 12 years [11]. Trana et al. conducted satellite remote sensing measurements of the heat island effect of 18 megacities located in both temperate and tropical regions in Asia. The focus of the analysis is on the correlation between the distribution of heat island effects and underlying surface types [12]. In 1982, Oke summarized and analyzed the early results of the UHI effect, including the intensity, spatial distribution, and influence factors of the heat island effect [13]. More than 20 years later, Arnfield reviewed the field since 1980 and summarized the turbulence model, urban microclimatic heat, and mass transfer model, and so forth, which are needed in the study of the UHI effect [14]. A recent review published by Mirzaei and Haghighat analyzed the theoretical models of the UHI effect in detail, particularly their effectiveness and limitations. Specific theoretical models include an energy balance model, a computational fluid dynamics model, a mesoscale model, a microscale model, and turbulence treatment [15]. Shi et al. continuously observed the temperature and humidity of soil in urban and rural areas and found that urban soils generally have higher temperatures and lower humidity than rural soils [16]. Yang et al. monitored the climate of 10 communities in Nanjing in three years and found that local climate changes have varying degrees of impact on residential and office buildings. [17]. Yao et al. standardized the temperature observed on-site in Nanjing under different weather conditions and evaluated the accuracy of the UHI diagnostic equation [18]. Using Landsat remote sensing images from 1988 to 2011 as the data source, Du et al. studied the temporal and spatial changes of the surface temperature obtained from the inversion [19].

Research on the relationship between the urban underlying surface and the UHI effect is abundant and involves various fields. Qiao et al. used Beijing Landsat thematic mapper (TM)/enhanced thematic mapper plus (ETM) data from 1989 to 2010 to analyze the effect of urban expansion's influence on the UHI [20]. Zhao and Jing analyzed the process of urbanization in Nanjing by using the analytic hierarchy process and the nonlinear fitting method. They selected the annual average maximum and minimum temperature as the research objects and discussed the relationship between urbanization and the urban temperature increase. Based on the data, a linear model of urbanization effect and temperature change is established [21]. Kong et al. analyzed the effect of green space pattern on heat dissipation in the eastern part of China, which showed that the cooling effect of urban green patches was becoming more and more important in rapid urban expansion. It provided a good theoretical and practical perspective for understanding the cool island effect of an urban green space in the urban area [22]. Based on the research on the Pearl River Delta, Peng et al. found that the cooling effect of the water body is not only related to the size of the area, but also related to the economic development of the region [23]. Yang forecasted the impact of different surface types on urban thermal environments via the Envi-met model [24]. Su et al. extracted the land surface temperature and land cover type of Landsat images in 2005 and analyzed their correlation [25]. Taking the Nanjing metropolitan area as the research area, Min et al. explored the impact of human activities and surface types on the UHI at different scales [26]. Yang et al. performed a numerical simulation of the cooling load of typical office buildings and apartment buildings to assess the impact of the UHI on building cooling load [27].

Finally, remote sensing provides an effective method for big data measurement of urban expansion and the heat island effect. Advanced very high-resolution radiometer (AVHRR) data from the National Oceanic and Atmospheric Administration (NOAA), thermal infrared (TIR) data from the thematic mapper (TM) and enhanced thematic mapper plus (ETM), and moderate-resolution imaging spectroradiometer (MODIS) LST products have been successively utilized to study the UHI effect. Landsat TM/ETM+ images are common data sources for impervious surface area mapping at regional

and even national scales [28–30]. For example, they have been used for developing national impervious surface area data in the USA [30]. Taubenböck et al. used Landsat images from 1975, 1990, 2000, and 2010 to examine 27 metropolis urban expansions [31]. Xie et al. applied a single-window algorithm to retrieve land-surface temperature and carried out background planning based on the UHI effect [32]. Zhou et al. studied the distribution of the urban thermal field using remote sensing and GIS [33].

Through the above analysis, it can find that many researches on urban underlying surfaces and the UHI have made a solid foundation for the follow-up study. However, less relevant research on underlying surface and the UHI effect has been done from a qualitative and quantitative level of Nanjing city. This proves the necessity and urgency of carrying out the research.

3. Methodology

3.1. Data Sources

Currently, the remote sensing data that has been frequently used in urban underlying surface research includes images provided by NOAA/AVHRR, Landsat, MODIS, and ASTER. Among various data sets used, Landsat images have been extensively applied in urban underlying surface research for their high-resolution images and easy to acquire data. Many of these studies have achieved fruitful research findings, such as [31]. As a result, this paper selects and analyses Landsat data from ten nonsequential years between 1984 and 2013.

Landsat series data can be downloaded for free from the website of the United States Geological Survey (USGS) after registration. The satellite remote sensing data used in this research is from the Landsat TM dataset, which was collected by second-generation Landsat satellites. In addition, the historical trend of air temperature urban heat island and surface temperature urban heat islands is analyzed by using the measured air temperature data in Nanjing over the ten years. The data, which was provided by Nanjing Meteorological Data Service Center, was obtained from an urban station (north latitude 31°95′′ and east longitude 118°85′′) and a rural station (north latitude 32°37′′ and east longitude 118°85′′). These two stations belong to the same district of Nanjing and have similar climatic characteristics.

3.2. The City of Nanjing and Data Selection

Nanjing, the capital city of Jiangsu province, China, is the subject city for the study. It is a major city in the region of Yangtze River Delta with a population of 9 million. Nanjing is in the lower reaches of the Yangtze River, surrounded by mountains. Nanjing is very rich in natural landscapes such as the Purple Mountains, Xuanwu Lake, Mochou Lake, and Qinhuai River Scenic Belt, for example. The geographical coordinates of Nanjing are between north latitude 31°14′′ and 32°37′′ and east longitude 118°22′′ and 119°14′′. These coordinates can be input into the website of USGS to obtain Landsat single-scene remote sensing images and data of Nanjing.

Note that the Landsat single-scene image covers an area of 180 × 180 km, which is significantly larger than the size of Nanjing. Therefore, the image needs to be cropped to fit the coordinates of Nanjing. Figure 1 shows the location of Nanjing and the Landsat remote sensing image of the studied area.

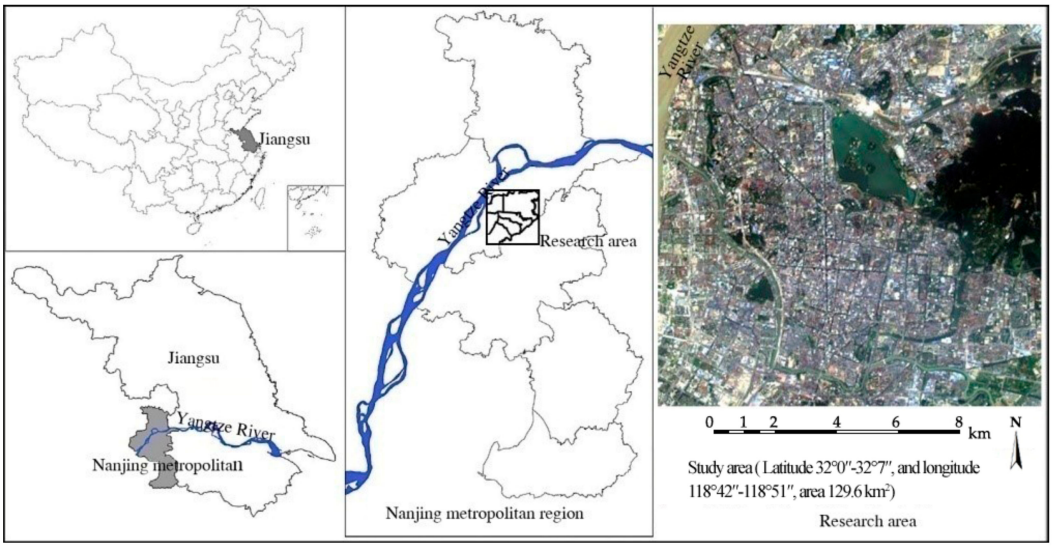

Figure 1. Location of Nanjing and the Research Area.

From the year of 1984 to 2018, only ten years' data were selected for analysis in this study for the following two reasons. Firstly, the quality of satellite remote sensing images is greatly affected by the weather. If the cloud cover is too large, the remote sensing image cannot be used to extract the underlying surface information. Secondly, the scan line corrector (SLC) of Landsat 7 failed after 31 May 2003. These products of Landsat 7 ETM+ have data gaps, so Landsat 7 ETM+ SLC-off data from the year of 2004 to 2007 has not been analyzed in this research. A summary of satellite images is shown in Table 1.

Table 1. A summary of satellite images from the year 1984 to 2018.

Year	Analyzed (Y)/Not Analyzed (N)	Months of Clear Images	Spatial Resolution (m)	Bands	Scene Information
1984	Y	7	80	4	The image of July is clear.
1985	N	11	80	4	There are clouds in the image of July.
1986	N	2	80	4	Only the image of February is clear.
1987	N	9, 12	80	4	There are clouds in the image of June.
1988	Y	7	80	4	The image of July is clear.
1989	N	3, 11, 12	80	4	The image of July cannot be obtained.
1990	Y	7	80	4	The image of July is clear.
1991	N	6, 8	80	4	There are clouds in the image of July.
1992	N	3, 10	80	4	The image of March and October is clear.
1993	N	2, 3, 11	30	7	The image of July cannot be obtained.
1994	Y	5, 6, 7	30	7	The image of July is clear.
1995	N	1, 3, 10	30	7	There are clouds in the image of July.
1996	N	2, 4, 12	30	7	The image of July cannot be obtained.
1997	N	10, 11	30	7	The image of October and November is clear.
1998	N	1, 2, 4, 5, 11, 12	30	7	The image of July cannot be obtained.
1999	N	5, 6, 12	30	7	The image of July cannot be obtained.
2000	Y	2, 4, 5, 7, 10	30	7	There are clouds in the image of July.
2001	Y	1, 2, 7, 10	30	7	There are clouds in the image of July.
2002	Y	3, 7	30	7	The image of July is clear.
2003	Y	1, 2, 3, 7, 10, 11	30	8	The image of July is clear.
2004	N	2, 7, 10, 11, 12	30	8	The image of July is ETM+ data, which has bands.
2005	N	10	30	8	Only the image of October is clear.
2006	N	4, 5, 7	30	8	The image of July is ETM+ data, which has bands.
2007	Y	1, 3, 5, 6, 7, 9	30	8	The image of July is clear.
2008	N	7, 9	30	8	The image of July is ETM+ data, which has bands.
2009	N	6, 10	30	8	The image of June and October is clear.

Table 1. *Cont.*

Year	Analyzed (Y)/Not Analyzed (N)	Months of Clear Images	Spatial Resolution (m)	Bands	Scene Information
2010	N	8	30	8	The image of August is clear.
2011	N	7	30	8	The image of July is ETM+ data, which has bands.
2012	N	7	30	8	The image of July is ETM+ data, which has bands.
2013	Y	7	15	11	The image of July is Landsat8 data.
2014	N	10	15	11	The image of July is ETM+ data, which has bands.
2015	N	4, 6, 10, 11, 12	30	8	There are clouds in the image of July.
2016	N	1, 2, 3, 4, 12	15	11	There are clouds in the image of July.
2017	N	1, 2, 3, 11, 12	15	11	There are clouds in the image of July.
2018	N	2, 4, 6	15	11	There are clouds in the image of July.

The major data processing methods in this research include an extraction of urban underlying surface types and land-surface temperature retrieval.

3.3. Classification of Urban Underlying Surfaces

The methods of processing satellite remote sensing data to extract urban underlying surface types include the Normalized Difference Vegetation Index method, decision tree method, supervised and non-supervised classification method, and so forth. In this research, the supervised classification method was adopted to process Landsat satellite remote sensing data, and the reasons for such a choice include the following: first, supervised classification can fully utilize the a priori knowledge of the classified region and determine the category of classification in advance; second, such a method can control the choice of training sample, and the accuracy of classification can be upgraded through repeated examinations of the training sample (to avoid a fatal error in classification); last, the supervised classification method can avoid the recapitulation of spectral cluster groups, which is required in non-supervised classification.

In this research, a supervised classification method was adopted to conduct image classification and extraction by using ENVI (v5.1) software. Supervised classification, also known as training ground classification, is used in the process of identifying unknown pixel types among the previously identified types of sample pixels. Before classification, through visual interpretation and field survey, a priori knowledge of the categorical attributes of the image surface features exists for some sample sections in the remote sensing image. As a result, training samples of each category are selected. Statistical information from each training sample section is determined via standard computer software, in addition to other information easily inferred from the data. The decision function is trained with these subcategory classifications to satisfy the requirements of various subcategory classifications. The final classification of the to-be-classified data is carried out using the trained decision function.

In this research, with the utilization of a supervised classification method, we conducted underlying surface extraction on the remote sensing data of Nanjing, which can be divided into the following three steps:

(a) Sample Selection

First, the remote sensing image was qualitatively divided into five categories, which included the river, lakes, forest and shrub vegetation, grass and agricultural lands, and impervious surface. After classification, samples were picked from areas of interest using the Region of Interest tool under the Overlay toolbar. After the sample selection, quantitative or qualitative verification was carried out on the samples with the Compute ROI Separability tool under the Options toolbar.

(b) Supervised Classification

Samples with a separation coefficient larger than 1.8 were deemed as qualified samples. Supervised classifications were carried out on qualified samples with the Supervised tool under the Classification toolbar.

(c) Process after Supervised Classification

Before it can be put into use, the results of supervised classification underwent additional meticulous processing, including the modification of the color and name (quality) of the classified results, modification of the wrongly classified categories (quality), majority/minority analysis (quality), and clump classes and sieve classes (quantity).

3.4. Retrieval of Urban Surface Temperature

Currently, there are mainly three methods of land-surface temperature retrieval with the utilization of the data of Landsat TM band 6, which include the mono-window algorithm method, atmospheric correction method, and generalized single-channel algorithm [34]. In the mono-window algorithm method, atmospheric effects are deduced via the equation; therefore, the atmospheric simulation can be converted into an algorithm but also eliminates the influence of atmospheric simulation error. Considering the condition of the acquired data and research into the region, the paper adopted a mono-window algorithm method to retrieve the land-surface temperature in Nanjing.

Before land-surface temperature retrieval, the Band Math tool in the ENVI software was introduced first. The Band Math tool can conveniently conduct mathematical function calculations, including addition, subtraction, multiplication, division, trigonometric function, index, and logarithm, as well as the functions written with IDL, of each band in the image. The functions that used Band Math tool were all data array operators based on IDL.

Different from single-channel algorithms and atmospheric correction, mono-window algorithms can directly retrieve land-surface temperature based on the land-surface thermal radiation conduction function without atmospheric correction. After the three parameters of atmospheric equivalent temperature T_a, atmospheric transmissivity T_6, and land-surface emissivity ε_6 are worked out, Equation (1) can be used to retrieve land-surface actual temperature according to planet brightness temperature (T_6) [22].

$$T_s = \{a_6(1 - C_6 - D_6) + [(b_6 - 1)(1 - C_6 - D_6) + 1]T_6 - D_6T_a\}/C_6 \quad (1)$$

where T_s is the land-surface actual temperature, in K; a_6 and b_6 are constant, and when the land-surface temperature is within the range of 0–70 °C, $a_6 = -67.355351$, and $b_6 = 0.458606$; T_a is the atmospheric equivalent temperature; and T_6 is the planet brightness temperature.

In this research, the above principles and methods were adopted to process the Landsat 5 TM remote sensing data of band 6, and the land-surface temperature data retrieved in ENVI was uploaded into ArcMap, which generated the retrieved image of land-surface temperature as shown in Figure 2. From the figure, it is easy to see that the lowest temperature of the retrieved region is 22.34 °C, and the highest is 35.12 °C. Such a remote sensing image has a resolution ratio of 30 m, each pixel containing one temperature data.

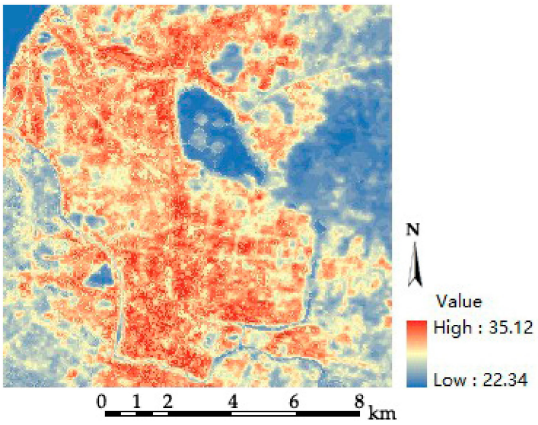

Figure 2. Results of land-surface temperature retrieval of Nanjing on 6 July 1990.

3.5. Determination of Urban and Rural Areas

After the acquisition of urban underlying surface type by using the supervised classification and mono-window algorithm method, respectively, GIS (Geographic Information System) was adopted for data processing to determine the relationship between urban underlying surface and UHI effect.

Due to the close interaction between remote sensing image analysis software ENVI and ArcMap, the data conversion between the two software methods is easy and convenient [35]. Remote sensing and GIS have a natural connection, and ArcGIS (v10.2) fully supports ENVI's raster file format. Meanwhile, ENVI fully supports the *.shp vector file format. Based on the integrative development of the two softwares, the results processed in ENVI could be directly sent to ArcMap via a menu.

After the results of supervised classification in ENVI were imported into GIS, due to the different resolution ratios among Landsat series satellite, these ten digital images were displayed in different areas, and the same geographic location could not overlap. To solve this problem, ArcGIS provides an effective method for geo-referencing. With the utilization of the geo-referencing tool, corresponding points of the two digital images were selected, and by means of setting controlling points, the matching of geographic locations of the two digital images could be achieved. The software was notified when the selected referencing points were as accordant as possible, and the accuracy of referencing points could be controlled through the observation of reference point residual errors. After geo-referencing, for the convenience of analysis, the images were cut into regions of the same size in accordance with extraction by mask. In ArcGIS, Conversion tools were used to convert raster data into vector data. This was done to further work out the proportion of different underlying surface types and their corresponding land-surface inversion temperature.

Moreover, the UHI is the difference between urban temperature and rural temperature. In this research, urban and rural areas need to be defined in the study area first. Nanjing was the national capital during the Six Dynasties, and the area within the ancient city walls was the location of imperial city since ancient times. The research area was already an urban area prior to 1984. Hence, the ratio of impervious surfaces inside the city walls annually is taken as the standard, as shown in Table 2. This standard is also used to divide rural and urban areas beyond the city wall. Such remote sensing images have a resolution ratio of 30 m. The research area was divided into a grid composed of 300 × 300 m square cells. First, the ratio of impervious surfaces inside city walls was calculated as shown in Table 2. If the ratio of the grid beyond the city walls was more than the ratio of impervious surfaces inside te city walls, it was defined as urban area. Otherwise, it was defined as rural area, as Figure 3 shows. By analyzing the high-resolution remote sensing map of the study area in corresponding years, it appears that the accuracy of this method is satisfactory.

Table 2. Statistics of the ratio of impervious surfaces inside city walls in the ten years.

Year	1984	1988	1990	1994	2000	2001	2002	2003	2007	2013
Ratio (%)	64	58	65	67	78	70	81	76	74	78

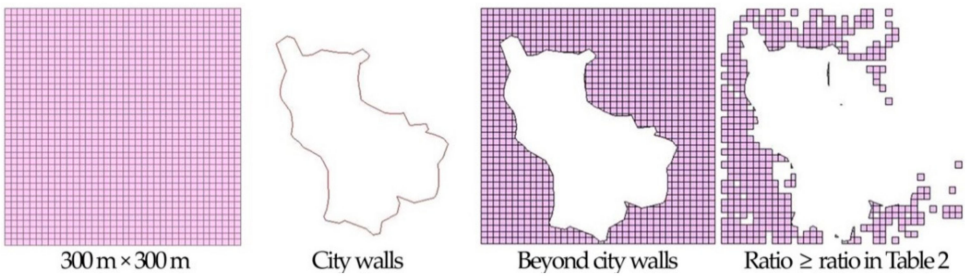

Figure 3. The definition of urban and rural areas divided by GIS.

The remaining Ming Dynasty City Wall divides the city of Nanjing into an inner city and an outer city. The inner-city area has a high ratio of impervious surfaces and is generally considered urban. The

method mentioned above is used to distinguish urban areas from rural areas. The result is shown in Figure 4.

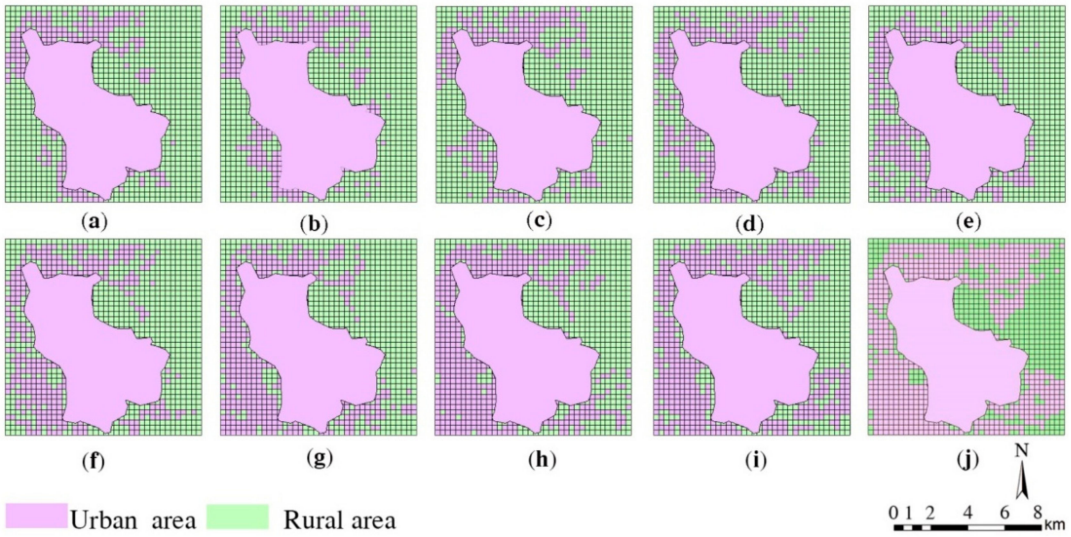

Figure 4. Urban and Rural Areas of the Ten Years Divided by GIS: (**a**) Urban and rural area of 1984; (**b**) Urban and rural area of 1988; (**c**) Urban and rural area of 1990; (**d**) Urban and rural area of 1994; (**e**) Urban and rural area of 2000; (**f**) Urban and rural area of 2001; (**g**) Urban and rural area of 2002; (**h**) Urban and rural area of 2003; (**i**) Urban and rural area of 2007; (**j**) Urban and rural area of 2013.

3.6. Urban Heat Island Effect Calculation

After the rural and urban areas are divided, the UHI is then calculated by GIS, based on Equations (2) and (3).

$$T_{UHI} = T_{Urban} - T_{Rural} \quad (2)$$

$$T_i = \frac{\sum_1^n T_i}{n} \ (i = 1, 2, 3 \ldots) \quad (3)$$

where T_{UHI} is the value of the UHI, T_{Urban} is the average temperature of urban areas, T_{Rural} is the average temperature of rural areas, T_i denotes the temperature of the i-th grid cell, and n is the number of the grid.

4. Results, Analysis, and Discussion

4.1. The General Pattern of Historical Changes of Nanjing's Urban Underlying Surface in the Last 30 Years

The study analyzed a total of 10 years of data concentrated around July, annually, because the heat island effect is significant in that period. The clear remote sensing image of that month can be acquired for more years. The remote sensing images in 2004, 2006, 2008, 2011, and 2012 are also clear. The images obtained after Landsat 7 were unfortunately degraded and repaired with an estimated value, so this study did not analyze them.

With the comprehensive utilization of supervised classification methods in ENVI and geo-referencing and extraction by mask methods in ArcGIS, the urban underlying classification results of the years 1984, 1988, 1990, 1994, 2000, 2001, 2002, 2003, 2007, and 2013 were achieved, as shown in Figure 5. From the urban underlying classification results of these ten years, the temporal changes in elevation of the urban underlying surface of Nanjing can be observed visually. The extension process of Nanjing's urban land use is witnessed by the ten years' supervised classification results of urban underlying surface by time sequence. The changes in Nanjing's urban underlying surface can be divided into the following phases by time sequence:

(1) From 1984 to 1990, the extension of Nanjing's impervious surface was mainly concentrated within the ancient city walls, with the characteristic lapping development and "filling the blanks in turn" [6], and the spatial growth mostly extended eastward along the Zhongshan Road and northward along the North Zhongshan Road, as shown in Figure 5a–c. The area of trees and shrubs reduced dramatically in the Purple Mountain region.

(2) From 1990 to 2001, the urban areas of Nanjing began to extend towards the outskirts of the ancient city. The urban canopy veins formed by roadside trees along South Zhongshan Road, Zhongshan Road and North Zhongshan Road within the old city became increasingly clear, as shown in Figure 5d–f. In the southwest direction, namely, the region to the west of Qinhuai River, large-scale construction was focused on areas from Jiangdong Gate to Jiangzhou. The region to the west of the Qinhuai River was one of the primary new areas of Nanjing's urban construction. From 1984 to 2001, the green and farmland area in west-river region dropped dramatically and was replaced by impervious surfaces in a large scale.

(3) From 2001 to 2013, there were still patches of trees and shrubs in the southern region of Xuanwu Lake and the western region of Yue-ya Lake in 2001. In the following 13 years, the area of green surfaces reduced, while the area of impervious surfaces increased, as shown in Figure 5g–j. The urban areas of Nanjing were continuously under eastward development along the Shanghai–Nanjing Highway.

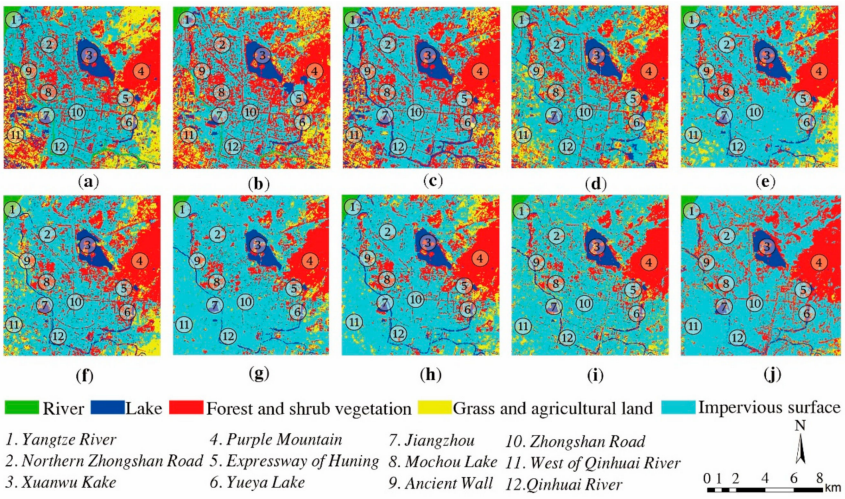

Figure 5. Results of supervised classification: (**a**) supervised classification result of 1984; (**b**) supervised classification result of 1988; (**c**) supervised classification result of 1990; (**d**) supervised classification result of 1994; (**e**) supervised classification result of 2000; (**f**) supervised classification result of 2001; (**g**) supervised classification result of 2002; (**h**) supervised classification result of 2003; (**i**) supervised classification result of 2007; (**j**) supervised classification result of 2013.

4.2. Quantitative Analysis on the Change Pattern of Different Underlying Surface Types

After the data was processed by GIS, quantitative analysis could be carried out to classify the results of underlying surface. In the analysis region of this research, the changes of water surfaces, green surfaces, and impervious surfaces are shown in Figure 6, and the ratio of these surfaces can be found in Table 3.

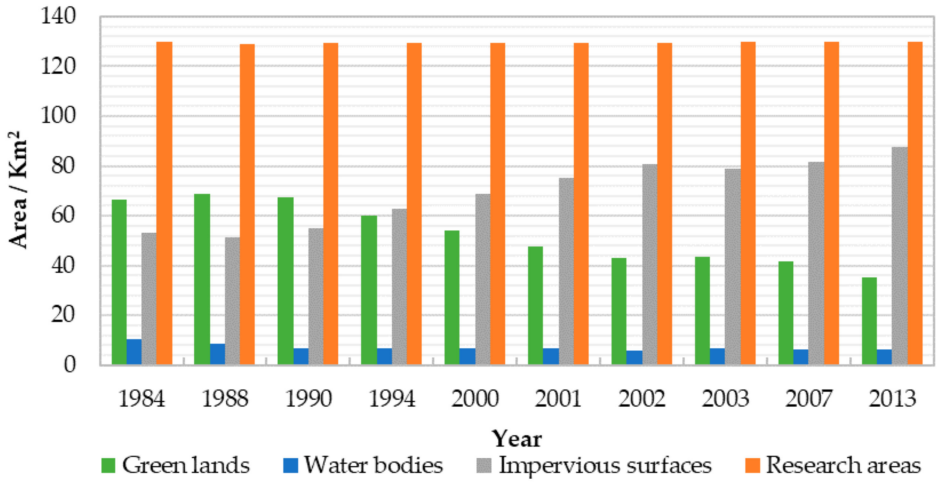

Figure 6. Results of supervised classification.

Table 3. Statistics of the ratio of green surfaces, water surfaces, and impervious surfaces in the ten years.

Year	Ratio of Green Surfaces (%)	Ratio of Water Surfaces (%)	Ratio of Impervious Surfaces (%)
1984	51.20	7.94	40.86
1988	53.74	6.63	39.63
1990	52.12	5.32	42.56
1994	46.41	5.17	48.42
2000	41.56	5.17	53.27
2001	36.63	5.47	57.90
2002	33.23	4.70	62.07
2003	33.61	5.40	60.99
2007	32.00	5.01	62.99
2013	27.37	5.01	67.62

(1) Quantitative analysis on green surface changes. From 1984 to 2013, due to the expansion of urban areas, the area of green surfaces in Nanjing reduced year by year gradually and dropped from what was 66.4 km^2 in 1984 to 35.5 km^2 in 2013. The ratio of green surfaces decreased by 23.83%.

(2) Quantitative analysis on water surfaces. From 1984 to 1990, the area of water surfaces in Nanjing experienced a 3.4 km^2 decline. Between 1990 and 2001, a 0.1 km^2 increase was seen. Between 2001 and 2007 a 0.5 km^2 decline was seen. From this data, it can be found that the change range of water surfaces area in Nanjing was no larger than 4.2 km^2 at any point in time between 1984 and 2013. After analyzing the area of water surface in Nanjing from 1984 to 2013, it can be concluded that the area of water surface in the analysis region basically remained unchanged.

(3) Quantitative analysis on impervious surfaces. From 1984 to 2013, the area of impervious surfaces in Nanjing witnessed a year-by-year growth, with a 2.1 km^2 increase from 1984 to 1990, a 20.0 km^2 increase from 1990 to 2001 and a 12.6 km^2 increase from 2001 to 2013. In the almost 30 years between 1984 and 2013, the area of impervious surfaces increased by 34.7 km^2, and the ratio of impervious surfaces increased by 26.76%.

4.3. The Pattern of Historical Changes of Nanjing's Urban Heat Island Effect in the Last 30 Years

4.3.1. The General Pattern of Historical Changes of Nanjing's Urban Heat Island Effect in the Last 30 Years

With the combined utilization of supervised classification methods in ENVI and geo-referencing and extraction by the mask method in GIS, the land-surface temperature retrieval of the years 1984, 1990, 1994, 2000, 2001, 2002, 2003, 2007, and 2013 was achieved, as shown in Figure 7. From the

land-surface temperature retrieval results of these ten years, it can be observed visually that the area of low temperature areas in Nanjing has witnessed dramatic changes. The changes of land-surface temperature can be divided into the following phases by time sequence:

(a) From 1984 to 1990, the areas of low temperature reduced, while the high-temperature areas expanded. In 1984, the high-temperature areas in Nanjing were mainly concentrated in the northwest part of the analysis region. The temperature in the west-river region and region to the south of the city wall concentrated between 15 °C and 20 °C, which belongs to a medium-temperature area, as shown in Figure 7a–c. The perimeter areas of Xuanwu Lake, Purple Mountain, and Yue-ya Lake belong to low-temperature areas. From 1984 to 1990, the region to the south of the city wall witnessed a change from a medium-temperature area to a high-temperature area, and the high-temperature areas outside the city wall gradually expanded along the perimeter of Mochou Lake.

(b) From 1990 to 2001, the whole west-river region witnessed a change from a low-temperature area to a high-temperature area, while the high-temperature areas around Beigu Mountain expanded and the low-temperature areas around Purple Mountain witnessed a corresponding decline. The low-temperature areas around Yue-ya Lake and the Shanghai-Nanjing Highway gradually reduced, as can be seen in Figure 7d–f.

(c) From 2001 to 2013, the pattern of low-temperature areas and high-temperature areas in the analysis region in Nanjing were generally stable and witnessed no obvious change, as shown in Figure 7g–j.

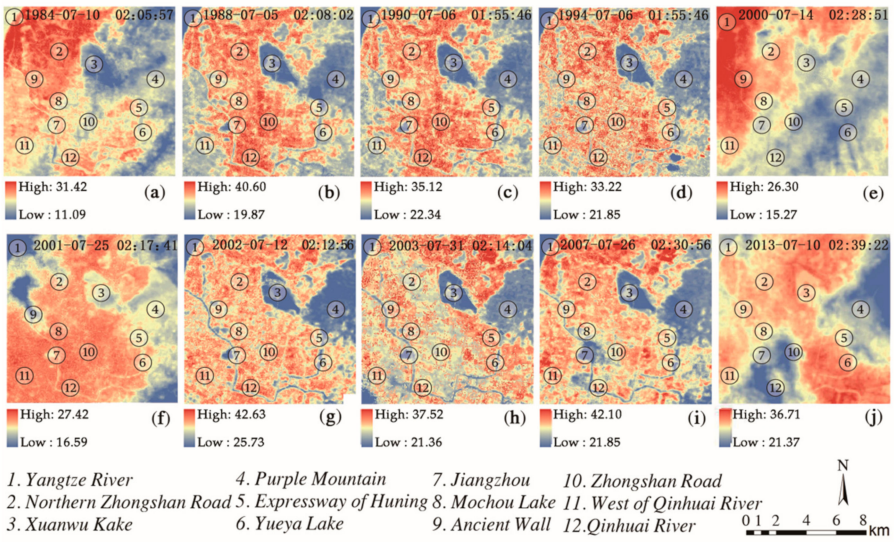

Figure 7. Retrieving land-surface temperature of the ten years: (**a**) retrieving land-surface temperature in 1984; (**b**) retrieving land-surface temperature in 1988; (**c**) retrieving land-surface temperature in 1990; (**d**) retrieving land-surface temperature in 1994; (**e**) retrieving land-surface temperature in 2000; (**f**) retrieving land-surface temperature in 2001; (**g**) retrieving land-surface temperature in 2002; (**h**) retrieving land-surface temperature in 2003; (**i**) retrieving land-surface temperature in 2007; (**j**) retrieving land-surface temperature in 2013.

4.3.2. Quantitative Analysis on the Pattern of Historical Changes of Nanjing's Urban Heat Island Effects in the Last 30 Years

After the data were processed by GIS, quantitative analysis could be carried out on the results of land-surface temperature retrieval. Within the analysis region of this research, the changes of temperatures in the past years can be seen in Figure 8. From 1984 to 2002, the average temperatures of both urban areas and suburban areas witnessed an upward tendency year by year, with the average temperature of urban areas rising from 32.99 °C in 1984 to 36.18 °C in 2002, and the average temperature

of suburban areas rising from 29.88 °C in 1984 to 32.37 °C in 2002. From 2002 to 2013, the average temperature of urban areas and suburban areas dropped from 36.18 °C to 33.76 °C and from 32.37 °C to 30.14 °C, respectively, the change range of which was relatively small and basically remained stable.

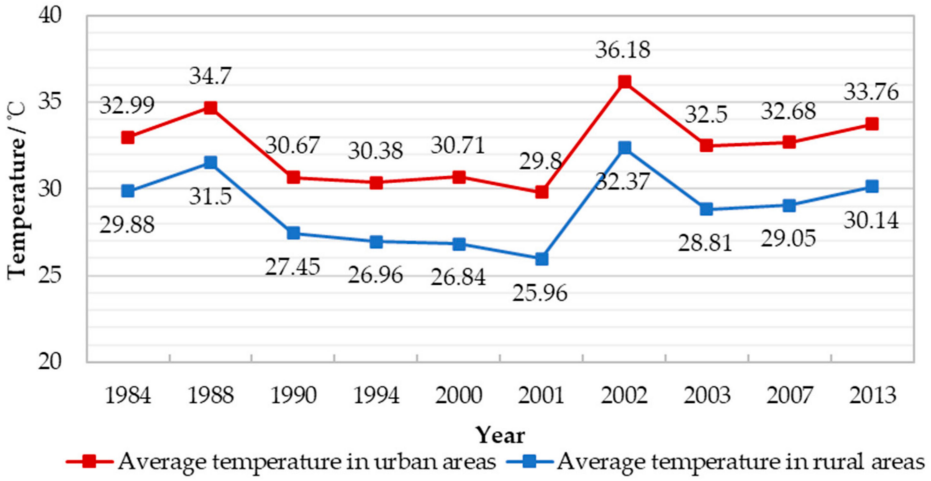

Figure 8. Average temperature in rural and urban areas.

The heat island intensity can be calculated, as shown in Figure 9. From 1984 to 2013, the intensity of the UHI changed from what was 3.11 °C in 1984 to 3.22 °C in 1990, from that of 3.22 °C in 1990 to 3.84 °C in 2001, and from 3.84 °C in 2001 to 3.62 °C in 2013, revealing an overall upward tendency. There was a decrease in the UHI effect after 2000. By analyzing relevant research findings, the reason for the decrease of heat island intensity in summer in Nanjing was that the local governments paid attention to the construction of green belts, parks, or environmental protection in the built-up areas, and the heat island effect in summer was alleviated [36].

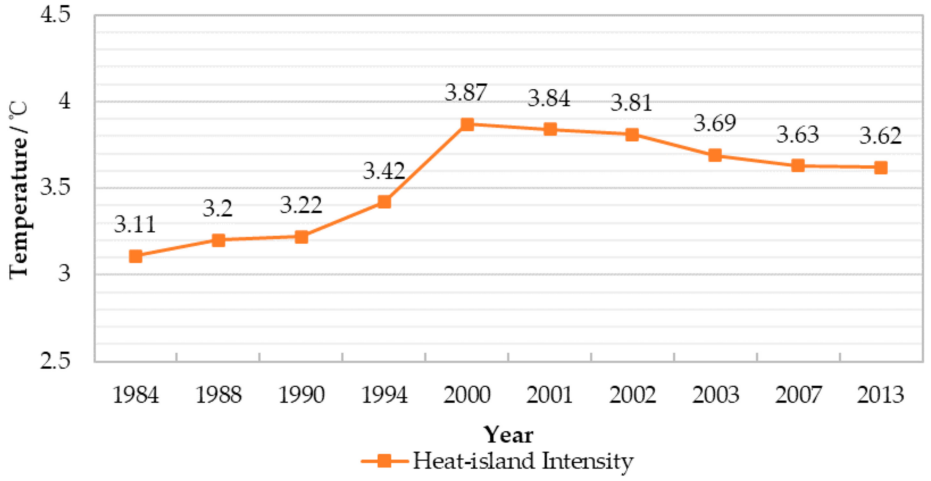

Figure 9. Heat island intensity of the ten years.

4.4. The Correlation between the Urban Underlying Surface and Nanjing's Urban Heat Island Effect in the Last 30 Years

In this paper, the variation law of an urban underlying surface and the UHI effect from 1984 to 2013 is studied and then the coupling relationship between them is explored. In the study of the variation of the urban underlying surface, it can be found that the rate of water area changed little in 30 years, only approximately 4 km^2, while the area of the green surface and impervious surface varied greatly, by more than 30 km^2. Therefore, this paper only considered green and impervious areas when analyzing the correlation between them.

To better explore the relationship between an UHI and an urban underlying surface, this paper displays the 10-year analysis data using a three-dimensional scatter plot, as shown in Figure 10. From the scatter plot, the correlation between the UHI and the urban underlying surface is not just a linear equation.

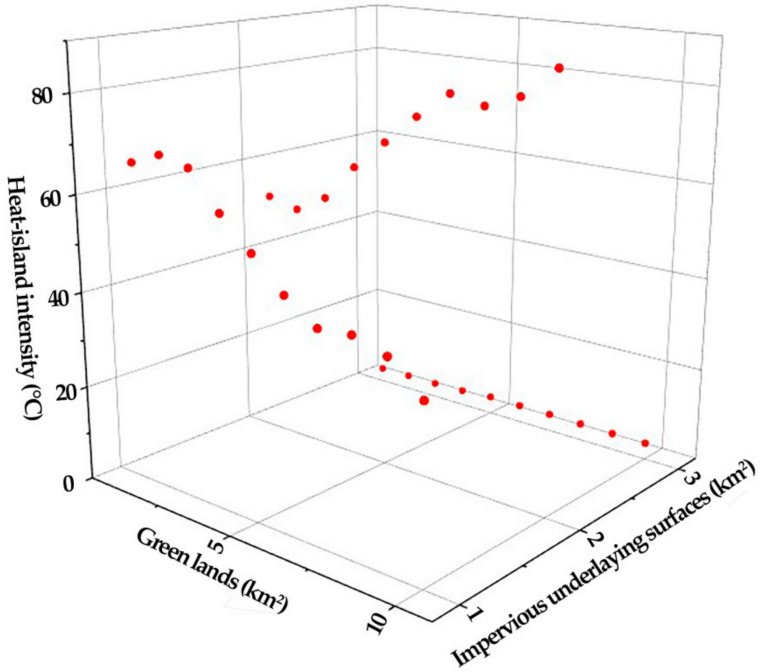

Figure 10. Three-dimensional scatter plot of heat island intensity, green and impervious surfaces areas.

Firstly, the relationship between the green area and UHI effect, and the relationship between the area of impervious surface and UHI effect were studied separately, as the former two charts in Figure 11 show. By polynomial fit, the relationships between an UHI effect and green area, or between an UHI effect and impervious surface area can be expressed by Equations (4) and (5), respectively.

$$y = 0.581 + 0.136x - 0.01x^2 \quad (4)$$

$$y = -2.850 + 0.175x - 0.01x^2 \quad (5)$$

Then, with the data of ten years, using the nonlinear regression statistical method, the relationship between the urban underlying surfaces was determined, and the UHI effect can be expressed by factors of these surfaces' area as shown in Equation (6).

$$y = -1124.98 + 19.40x_1 + 17.67x_2 - 0.08x_1^2 - 0.07x_2^2 \quad (6)$$

In the equation, y is the UHI effect, x_1 is the green area, and x_2 is the area of impervious surface. In the regression equation, the complex correlation coefficient is R, and R equals 0.9612, which indicates that the relationship between them is highly correlated. The complex determination coefficient, or the square of R, was used to explain the degree of variation of the dependent variable y; this was done to determine the fitting effect of the dependent variable y. As shown in Table 4, the complex determination coefficient in this regression equation is 0.9238, indicating that 92.38% of the variance of the dependent variable can be explained by using the independent variable. The adjusted R squared value is the adjusted complex coefficient of R^2, which is 0.8286, indicating that the independent variable can account for 82.86% of the dependent variable y, and 17.14% of the variable y is interpreted by other factors. The standard error was used to measure the degree of the fit and to calculate the other statistics associated with the regression. The smaller the value is, the better the degree of fitting is. The

standard error of the regression equation was 0.1176, and this is a good result. In the linear regression analysis, the main function of the "variance analysis table" was to determine the regression effect of the regression model via an *F* test. The *P*-value of the significance *F* (*F* is statistically significant) in the regression equation was 0.023471, which is less than the significance level of 0.05. The regression equation had a significant regression effect, and at least one regression coefficient in the equation was not 0, which is also significant. *P*-value is the *P*-value of the regression coefficient *t* statistic. As shown in Table 5, it is worth noting that the *P*-parameter of the *t*-statistic of the independent variable was 0.22, 0.23, 0.22, 0.21, and 0.23, which was less than the significance level of 0.25; this means that the independent variable has a strong correlation with y, and the regression coefficient is significant.

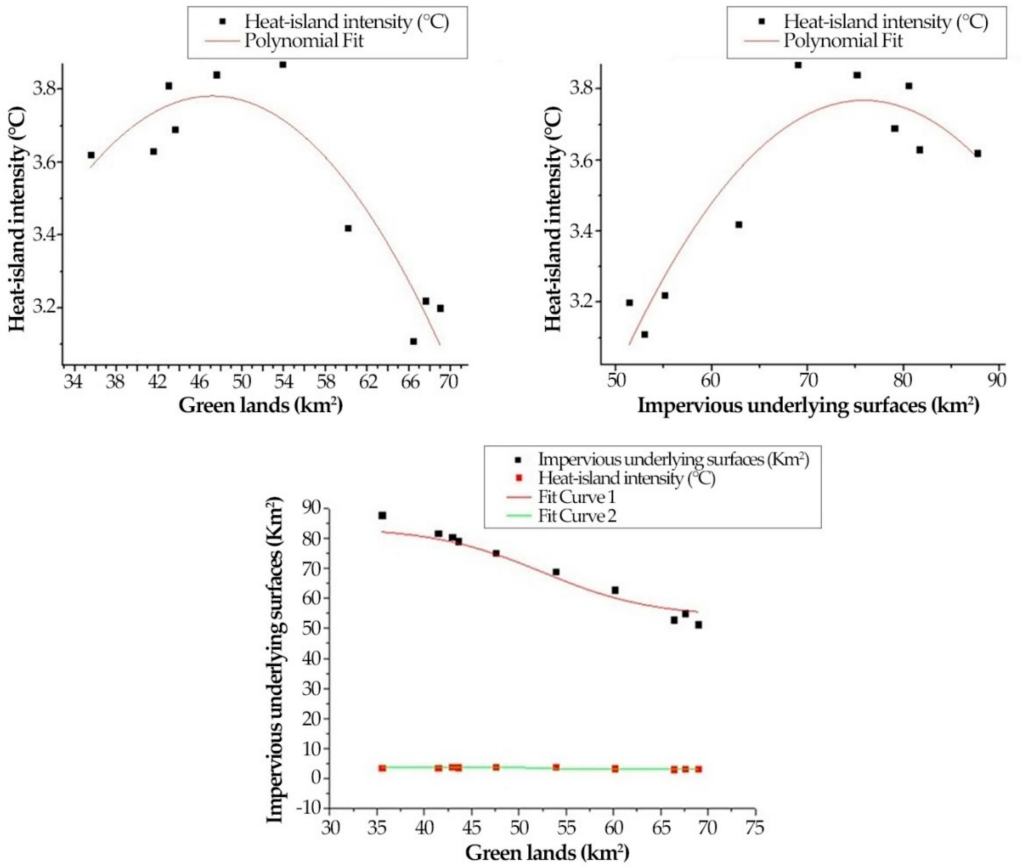

Figure 11. The correlation between the underlying surfaces and UHI intensity of the ten years.

Table 4. Table for linear regression analysis.

Multiple Correlation Coefficient *R*	*R* Square	Adjusted *R* Square (R^2)	Significance *F*
0.9612	0.9238	0.8286	0.023471

Table 5. Test of regression coefficient of nonlinear regression equation.

Coefficient	Value	*T* Value	*P* Value
Intercept	−1125.98	−1.4	0.22
X Variable 1	19.40	1.5	0.22
X Variable 2	17.67	1.4	0.23
X Variable 3	−0.15	−1.4	0.22
X Variable 4	−0.08	−1.5	0.21
X Variable 5	−0.07	−1.4	0.23

4.5. Air Temperature Urban Heat Island

The air temperature UHI is typically characterized by air temperature, while the surface temperature UHI is reflected by surface temperature [37]. The combination of air temperature and land-surface temperature would add value in exploring UHI effects [38]. Yang et al. found that the surface UHI intensity was considerably stronger than that of air temperature in summer (the surface UHI was 6.83 °C and air temperature UHI was 0.27 °C). Meanwhile, this research also considers that the relationships between land-surface temperature and air temperature were all statistically significant [38].

Using the air temperature data provided by the Nanjing Meteorological Data Service Center, the historic trend of the air temperature UHI intensity from 1984 to 2013 was calculated and plotted, as shown in Figure 12. Note that the urban air temperature and the rural air temperature used to calculate the air temperature UHI were both the monthly average temperature in July.

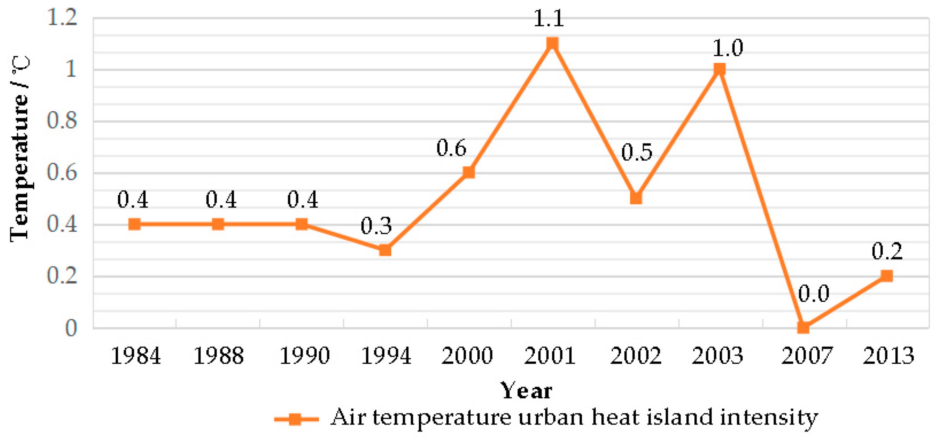

Figure 12. Air temperature urban heat island intensity of the ten years.

By comparing Figures 9 and 12, the following findings can be made:

(1) The measured data of the air temperature proves that the urban heat island effect in Nanjing is obvious. However, the surface temperature UHI intensity is generally stronger than the air temperature UHI intensity.

(2) The historical trend of the air temperature UHI intensity is similar to that of the surface temperature UHI intensity, i.e., they both show a pattern of increasing between 1984 and 2000 and decreasing after 2000. In the case of the air temperature UHI, the inversion occurred in 2001, slightly different from 2000.

5. Conclusions

Based on the qualitative and quantitative analysis of the underlying surface information and temperature information in different years, the following conclusions are drawn:

(1) From 1984 to 1990, the extension of impervious surfaces in Nanjing mainly concentrated within the ancient city walls. The spatial growth of impervious surfaces mostly extended eastward along the Zhongshan Road and northward along the North Zhongshan Road. The area of trees and shrubs reduced dramatically in the Purple Mountain region, with the area of green surfaces rising from 66.4 km^2 in 1984 to 67.6 km^2 in 1990 and the area of impervious surfaces increasing from 53.0 km^2 to 55.1 km^2. In the same period, the medium-temperature zone in the southern part within the city wall was replaced with a high-temperature zone. The high-temperature zone beyond the city wall extended along the perimeter of Mochou Lake. The average temperature of urban areas increased from 22.99 °C to 30.67 °C.

(2) From 1990 to 2001, the urban areas of Nanjing extended beyond the city wall rapidly. The urban canopy veins formed by the trees along the South Zhongshan Road, the Zhongshan Road, and the North Zhongshan Road became increasingly clear. From 1984 to 2002, the green and farmland areas in the west of Qinhuai river region dropped dramatically. The area of impervious surfaces increased from 67.6 km^2 to 75.1 km^2. In addition, the whole west-river region witnessed a change from low temperature to high temperature, while the high-temperature areas around Beigu Mountain expanded, and the low-temperature areas around Purple Mountain witnessed a corresponding decrease. The low-temperature areas around Yue-ya Lake and the Shanghai-Nanjing Highway gradually reduced. The UHI increased from 3.22 °C to 3.81 °C.

(3) From 2001 to 2013, the whole surface west of Qinghuai River and east along Shanghai–Nanjing Highway became an impervious surface after nearly 10 years. In 2002, there were still patches of trees and shrubs in the southern region of Xuanwu Lake and western region of Yue-ya Lake. In the years that followed until 2007, the area of green surfaces decreased 1.5 km^2, while the area of impervious surfaces increased 1.2 km^2. The urban areas of Nanjing were continuously growing eastward along the Shanghai-Nanjing Highway. In 2013, the overall urban spatial pattern remained stable. The pattern of low-temperature areas and high-temperature areas was also stable in general, and the intensity of the UHI changed from 3.81 °C to 3.62 °C.

In summary, it is obvious that Nanjing has undergone an urbanization process in the past 30 years with a 34.7 km^2 increase in the area of impervious surfaces, a 30.9 km^2 decrease in the area of green surfaces, and a relatively stable area of water surfaces. The extension of Nanjing's developed urban land reveals an overall tendency of "eastward spreading and southward translocation". The region to the west of Qinhuai River is one of the primary newly developed areas. At the same time, the low-temperature areas significantly reduced, and the high-temperature areas increased in Nanjing. The average temperature in the urban area increased by 0.77 °C, and the intensity of heat island increased by 0.51 °C. Based on the analysis of the effect of the underlying surfaces and the UHI in Nanjing, this paper puts forward the hypothesis that the urban underlying surface has a nonlinear relationship with the UHI effect.

The correlation between the transformation of underlying surfaces and the UHI in the city of Nanjing needs to be studied further. The following limits should be noticed for future research. The common UHI is the difference of temperature of the atmosphere, but the intensity of the UHI used the different temperature of the land surfaces. Furthermore, the canopy of trees is also influenced by seasons, so the area of underlying surfaces is changing constantly. The temperature of the underlying surface is influenced by the weather, even in the same month. Finally, this research was conducted during July for only ten years. Thus, further research is needed to compare to this study's conclusions.

Author Contributions: Conceptualization: Y.L. (Yanxia Li) and X.S.; methodology: Y.L. (Yanxia Li); software: Y.L. (Yanxia Li); validation: Y.L. (Yanxia Li), X.Z., S.Z., X.W., and Y.L. (Yanxia Li); investigation: Y.L. (Yanxia Li); data curation: Y.L. (Yongdong Lu); writing—original draft preparation: Y.L. (Yanxia Li); writing—review and editing: Y.L. (Yanxia Li), X.Z., S.Z., S.D., and X.S.; funding acquisition: X.S. All authors have read and agreed to the published version of the manuscript.

Funding: This paper is financially supported by the National Natural Science Foundation of China, grant number: 51678124.

Conflicts of Interest: The authors declare no conflict of interest.

References

1. Un-Habitat. *State of the World's Cities 2008/2009 Harmonious Cities*, 1st ed.; Routledge: London, UK, 2008; pp. 222–224. [CrossRef]
2. Kuang, W.H.; Chi, W.F.; Lu, D.S.; Dou, Y.Y. A comparative analysis of megacity expansions in China and the U.S.: Patterns, rates and driving forces. *Landsc. Urban Plan.* **2014**, *132*, 121–135. [CrossRef]
3. Kwak, Y.; Park, C.; Deal, B. Discerning the success of sustainable planning: A comparative analysis of urban heat island dynamics in Korean new towns. *Sustain. Cities Soc.* **2020**, *61*, 102341. [CrossRef]

4. Cai, Y.Y.; Mou, S.G.; Xiao, B.; Wang, Y.; Liu, P.X. Analysis on coordination degree between land use and urbanization level of Nanjing city. *J. Shandong Agric. Univ.* **2011**, *42*, 145–149.
5. Zhang, M.M.; Wang, Y.H.; Chai, M.T.; Li, D.L. Study on Relationship between Population Urbanization and Land Urbanization. *J. Anhui Agric. Sci.* **2011**, *39*, 17450–17452. [CrossRef]
6. Shi, X. Study on the Urban Using Land Expansion in Period of High-Speed Urbanization-A Case of Nanjing. Master's Thesis, Nanjing Agricultural University, Nanjing, China, 2004.
7. Wang, L.J. The Intensive Utilization of Urban Land During a Rapid Urbanization. Master's Thesis, Nanjing Agricultural University, Nanjing, China, 2006.
8. Tu, L.; Qin, Z.; Li, W.; Geng, J.; Yang, L.; Zhao, S.; Wang, F. Surface urban heat island effect and its relationship with urban expansion in Nanjing, China. *J. Appl. Remote. Sens.* **2016**, *10*, 26–37. [CrossRef]
9. Kolokotroni, M.; Giannitsaris, I.; Watkins, R. The effect of the London urban heat island on building summer cooling demand and night ventilation strategies. *Sol. Energy* **2006**, *80*, 383–392. [CrossRef]
10. Wang, Q.; Zhang, C.; Ren, C.; Hang, J.; Li, Y. Urban heat island circulations over the Beijing-Tianjin region under calm and fair conditions. *Build. Environ.* **2020**, *180*, 107063. [CrossRef]
11. Streutker, D.R. Satellite-measured growth of the urban heat island of Houston, Texas. *Remote Sens. Environ.* **2003**, *85*, 282–289. [CrossRef]
12. Hung, T.; Uchihama, D.; Ochi, S.; Yasuoka, Y. Assessment with satellite data of the urban heat island effects in Asian mega cities. *Int. J. Appl. Earth Obs. Geoinf.* **2006**, *8*, 34–48. [CrossRef]
13. Oke, T.R. The energetic basis of the urban heat island. *Q. J. R. Meteorol. Soc.* **1982**, *108*, 1–24. [CrossRef]
14. Arnfield, A.J. Two decades of urban climate research: A review of turbulence, exchanges of energy and water, and the urban heat island. *Int. J. Climatol.* **2003**, *23*, 1–26. [CrossRef]
15. Mirzaei, P.A.; Haghighat, F. Approaches to study Urban Heat Island: Abilities and limitations. *Build. Environ.* **2010**, *45*, 2192–2201. [CrossRef]
16. Shi, B.; Tang, C.; Gao, L.; Liu, C.; Wang, B. Observation and analysis of the urban heat island effect on soil in Nanjing, China. Environ. *Earth Sci.* **2012**, *67*, 215–229. [CrossRef]
17. Yang, X.; Peng, L.L.; Jiang, Z.; Chen, Y.; Yao, L.; He, Y.; Xu, T. Impact of urban heat island on energy demand in buildings: Local climate zones in Nanjing. *Appl. Energy* **2020**, *260*, 114–279. [CrossRef]
18. Yao, L.; Yang, X.; Zhu, C.; Jin, T.; Peng, L.; Ye, Y. Evaluation of a Diagnostic Equation for the Daily Maximum Urban Heat Island Effect. *Procedia Eng.* **2017**, *205*, 2863–2870. [CrossRef]
19. Du, L.; Zhou, T.; Li, M.; Gong, D. Urban heat island effects derived from dense Landsat thermal observations in Nanjing, China. IOP Conference Series. *Earth Environ. Sci.* **2014**, 17.
20. Qiao, Z.; Tian, G.J.; Zhang, L.X.; Xu, X.L. Influences of urban expansion on urban heat island in Beijing during 1989–2010. *Adv. Meteorol.* **2014**, *2014*, 1–11. [CrossRef]
21. Zhao, H.J.; Jing, Y.S. The Effect of Urbanization on Air Temperature Increase in Nanjing City. *J. Anhui Agric. Sci.* **2008**, *28*. [CrossRef]
22. Kong, F.H.; Yin, H.W.; James, P.; Hutyra, L.R.; Hong, S.H. Effects of spatial pattern of greenspace on urban cooling in a large metropolitan area of eastern China. *Landsc. Urban Plan.* **2014**, *128*, 35–47. [CrossRef]
23. Peng, J.; Liu, Q.; Xu, Z.; Lyu, D.; Du, Y.; Qiao, R.; Wu, J. How to effectively mitigate urban heat island effect? A perspective of waterbody patch size threshold. *Landsc. Urban Plan.* **2020**, *202*, 103873. [CrossRef]
24. Yang, X.S.; Zhao, L.H.; Bruse, M.; Meng, Q.L. Evaluation of a microclimate model for predicting the thermal behavior of different ground surfaces. *Build. Environ.* **2013**, *60*, 93–104. [CrossRef]
25. Su, W.; Gu, C.; Yang, G. Assessing the Impact of Land Use/Land Cover on Urban Heat Island Pattern in Nanjing City, China. *J. Urban Plan. Dev.* **2010**, *136*, 365–372. [CrossRef]
26. Min, M.; Lin, C.; Duan, X.; Jin, Z.; Zhang, L. Spatial distribution and driving force analysis of urban heat island effect based on raster data: A case study of the Nanjing metropolitan area, China. *Sustain. Cities Soc.* **2019**, *50*, 101–637. [CrossRef]
27. Yang, X.; Jin, T.; Yao, L.; Zhu, C.; Peng, L. Assessing the Impact of Urban Heat Island Effect on Building Cooling Load based on the Local Climate Zone Scheme. *Procedia Eng.* **2017**, *205*, 2839–2846. [CrossRef]
28. Lu, D.S.; Weng, Q.H. Use of impervious surface in urban land-use classification. *Remote Sens. Environ.* **2006**, *102*, 146–160. [CrossRef]
29. Wickham, J.D.; Stehman, S.V.; Gass, L.; Dewitz, J.; Fry, J.A.; Wade, T.G. Accuracy assessment of NLCD 2006 land cover and impervious surface. *Remote Sens. Environ.* **2013**, *130*, 294–304. [CrossRef]

30. Xian, G.; Homer, C. Updating the 2001 national land cover database impervious surface products to 2006 using Landsat imagery change detection methods. *Remote Sens. Environ.* **2010**, *114*, 1676–1686. [CrossRef]
31. Taubenböck, H.; Esch, T.; Felbier, A.; Wiesner, M.; Roth, A.; Dech, S. Monitoring urbanization in mega cities from space. *Remote Sens. Environ.* **2012**, *117*, 162–176. [CrossRef]
32. Xie, J.F.; Liu, T.T.; Guo, J. Application of single-window algorithm to urban planning of urban heat island effect in Beijing. *Gard. Sci. Technol. J.* **2011**, *122*, 7–11.
33. Zhou, H.M.; Zhou, C.H.; Ge, W.Q.; Ding, J.C. The Surveying on Thermal Distribution in Urban Based on GIS and Remote Sensing. *Acta Geogr. Sin.* **2001**, *68*, 189–197. [CrossRef]
34. Qin, Z.H.; Li, W.J.; Xu, B.; Chen, Z.X.; Liu, J. The estimation of land surface emissivity for Landsat TM6. *Remote Sens. Land Resour.* **2004**, *16*, 28–32. [CrossRef]
35. Xu, D.Q.; Tang, X.J.; He, Z. Information conversion between the remote sensing image software ENVI and GIS software. *J. Water Resour. Water Eng.* **2005**, *16*, 67–70.
36. Yan, S.; Zhang, J.; Zhang, B.; Lu, Q.; Wang, Y.; Yu, H.; Zhang, Z. Evolution of urban heat island effect in 2008 and its influence on resident life in Nanjing, Jiangsu province. *J. Meteorol. Environ.* **2011**, *27*, 14–20.
37. Oke, T.R. *Initial Guidance to Obtain Representative Meterorological Observations at Urban Sites*; University of British Columbia: Vancouver, BC, Canada, 2004.
38. Yang, C.; Yan, F.; Zhang, S. Comparison of land surface and air temperatures for quantifying summer and winter urban heat island in snow climate city. *J. Environ. Manag.* **2020**, *265*, 110–563. [CrossRef] [PubMed]